

# The Taiji-TianQin-LISA network: Precisely measuring the Hubble constant using both bright and dark sirens

Shang-Jie Jin,<sup>1</sup> Ye-Zhu Zhang,<sup>1</sup> Ji-Yu Song,<sup>1</sup> Jing-Fei Zhang,<sup>1</sup> and Xin Zhang<sup>1,2,3,\*</sup>

<sup>1</sup>Key Laboratory of Cosmology and Astrophysics (Liaoning) & College of Sciences,  
Northeastern University, Shenyang 110819, China

<sup>2</sup>Key Laboratory of Data Analytics and Optimization for Smart Industry (Ministry of Education),  
Northeastern University, Shenyang 110819, China

<sup>3</sup>National Frontiers Science Center for Industrial Intelligence and Systems Optimization,  
Northeastern University, Shenyang 110819, China

In the coming decades, the space-based gravitational-wave (GW) detectors such as Taiji, TianQin, and LISA are expected to form a network capable of detecting millihertz GWs emitted by the mergers of massive black hole binaries (MBHBs). In this work, we investigate the potential of GW standard sirens from the Taiji-TianQin-LISA network in constraining cosmological parameters. For the optimistic scenario in which electromagnetic (EM) counterparts can be detected, we predict the number of detectable bright sirens based on three different MBHB population models, i.e., pop III, Q3d, and Q3nod. Our results show that the Taiji-TianQin-LISA network alone could achieve a constraint precision of 0.9% for the Hubble constant, meeting the standard of precision cosmology. Moreover, the Taiji-TianQin-LISA network could effectively break the cosmological parameter degeneracies generated by the CMB data, particularly in the dynamical dark energy models. When combined with the CMB data, the joint CMB+Taiji-TianQin-LISA data offer  $\sigma(w) = 0.036$  in the  $w$ CDM model, which is close to the latest constraint result obtained from the CMB+SN data. We also consider a conservative scenario in which EM counterparts are not available. Due to the precise sky localizations of MBHBs by the Taiji-TianQin-LISA network, the constraint precision of the Hubble constant is expected to reach 1.1%. In conclusion, the GW standard sirens from the Taiji-TianQin-LISA network will play a critical role in helping solve the Hubble tension and shedding light on the nature of dark energy.

## I. INTRODUCTION

The precise measurements of the cosmic microwave background (CMB) anisotropies have ushered in the era of precision cosmology [1, 2]. Nevertheless, in recent years, with the improvements of the measurement precisions of cosmological parameters, some puzzling tensions appeared. In particular, the tension between the Hubble constant values inferred from the *Planck* CMB observation (a 0.8% measurement, assuming the  $\Lambda$ CDM model) [3] and obtained through the distance ladder method (a 1.4% measurement) [4] is now at the  $5\sigma$  level [4]. The Hubble tension is now commonly considered a severe crisis for cosmology [5, 6], which has been widely discussed in the literature [5–30]. The Hubble tension may herald the possibility of new physics beyond the standard model of cosmology. However, no consensus has been reached on a valid extended cosmological model that can truly solve the Hubble tension. On the other hand, it is crucial to develop cosmological probes that can independently measure the Hubble constant and make an arbitration for the Hubble tension. The gravitational-wave (GW) standard siren method is one of the most promising methods.

The absolute distance information of a GW source could be obtained by analyzing the GW waveform, which

is called a standard siren [31, 32]. If the redshift information could also be obtained from the associated electromagnetic (EM) counterparts (we usually refer to this kind of standard sirens as “bright sirens”), the established distance-redshift relation can then be used to explore the expansion history of the universe. The only multi-messenger observation event GW170817 has given the first measurement of  $H_0$  using the standard siren method, with about 14% precision [33]. The constraint precision of  $H_0$  is expected to be 2% using 50 similar standard siren events [34]. Although for the current detected stellar-mass binary black hole mergers their EM counterparts cannot be detected, the statistical method could be applied in inferring the redshift information for the cosmological parameter estimation (we usually refer to this kind of standard sirens as “dark sirens”; see e.g., Refs. [34–50] for related works). Recently, GW standard sirens have been widely discussed in the literature [51–90].

The GW detectors will be greatly developed in the next decades. For the detection of GWs in the frequency band of several hundred (up to several thousand) hertz, we will have the third-generation ground-based GW detectors, e.g., the Cosmic Explorer [91] and the Einstein Telescope [92], which are one order of magnitude more sensitive than the current GW detectors. They are expected to detect standard sirens with redshifts mainly distributed at  $z < 3$  [93]. The cosmological parameter estimations using the standard sirens have been forecasted in e.g., Refs. [94–100].

---

\*Corresponding author.  
zhangxin@mail.neu.edu.cn

The space-based GW detectors, Taiji [101–103], TianQin [104–109], and LISA [110–112], will open a window for detecting millihertz GWs emitted from the mergers of massive black hole binaries (MBHBs), extreme mass ratio inspirals, etc. According to recent forecasts, the mergers of MBHBs could emit EM radiations in both the radio and optical bands [113–120], which are expected to be observed by EM detectors, e.g., Square Kilometer Array (SKA) [121], the Extremely Large Telescope (ELT) [122], the Large Synoptic Survey Telescope (LSST) [123], etc. Compared to the single GW observatory, the GW detection network consisting of multiple GW observatories could improve the measurement precisions of GW parameters [124–129]. Recently, Ruan *et al.* [127] proposed that Taiji and LISA could form a space-based detector network. Compared to the single Taiji observatory, the Taiji-LISA network could greatly improve the ability to locate the GW sources, promoting the applications of the standard siren method in cosmological parameter estimations (related works could refer to e.g., Refs. [73, 125]).

In the coming decades, Taiji, TianQin, and LISA are expected to observe simultaneously and provided unprecedented high-accuracy localizations of MBHBs. Notably, studies on the cosmological parameter estimation using the standard sirens from the space-based Taiji-TianQin-LISA detector network are still absent. The aim of this work is to explore the potential of the Taiji-TianQin-LISA network in answering three key questions: (i) how well the Taiji-TianQin-LISA network can locate MBHBs, (ii) what precision the cosmological parameters can be measured by the bright sirens from the Taiji-TianQin-LISA network, and (iii) what precision the Hubble constant can be measured using the dark sirens from the Taiji-TianQin-LISA network. Through this work, we hope to deepen our understanding of the standard sirens from the Taiji-TianQin-LISA network for solving the Hubble tension and investigating the potential of measuring dark energy.

This work is organized as follows. In Sec. II, we introduce the methodology used in this work. In Sec. III, we detailedly introduce the simulations of bright and dark sirens. In Sec. IV, we give the constraint results and make some relevant discussions. The conclusion is given in Sec. V.

## II. METHODOLOGY

### A. Cosmological models

The luminosity distance of a source at redshift  $z$  can be written as

$$d_L(z) = c(1+z) \int_0^z \frac{dz'}{H(z')}, \quad (1)$$

where  $c$  is the speed of light in vacuum,  $H(z)$  is the Hubble parameter which describes the expansion rate of the universe at redshift  $z$ .

In this work, we consider the  $\Lambda$ CDM,  $w$ CDM, and  $w_0w_a$ CDM models to make cosmological analysis.

- $\Lambda$ CDM: the standard model of cosmology with the equation of state (EoS) parameter of dark energy  $w = -1$ . The form of  $H(z)$  is given by

$$H(z) = H_0 \sqrt{\Omega_m(1+z)^3 + 1 - \Omega_m}, \quad (2)$$

where  $\Omega_m$  is the current matter density parameter and  $H_0$  is the Hubble constant.

- $w$ CDM: the simplest case for dynamical dark energy model with  $w = \text{constant}$ . The form of  $H(z)$  is given by

$$H(z) = H_0 \sqrt{\Omega_m(1+z)^3 + (1 - \Omega_m)(1+z)^{3(1+w)}}. \quad (3)$$

- $w_0w_a$ CDM: a phenomenological model to explore the evolution of  $w$ . The forms of  $w(z)$  and  $H(z)$  are given by

$$w(z) = w_0 + w_a \frac{z}{1+z}, \quad (4)$$

$$H(z) = H_0 \sqrt{\Omega_m(1+z)^3 + (1 - \Omega_m)(1+z)^{3(1+w_0+w_a)} \exp\left(-\frac{3w_a z}{1+z}\right)}. \quad (5)$$

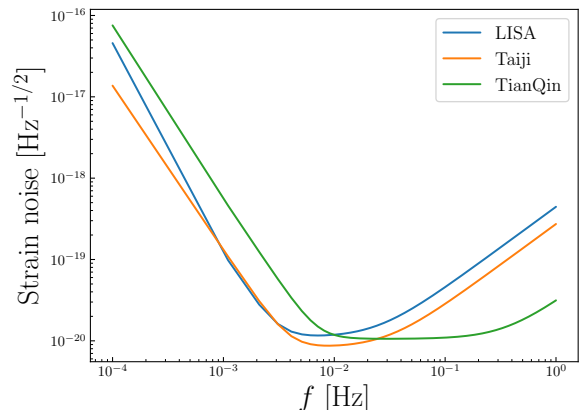


FIG. 1: The sensitivity curves of Taiji, TianQin, and LISA.

Throughout this paper, we adopt the flat  $\Lambda$ CDM model as the fiducial model to generate the mock standard siren data with  $\Omega_m = 0.3166$  and  $H_0 = 67.27 \text{ km s}^{-1} \text{ Mpc}^{-1}$  from the constraint results by the *Planck* 2018 TT,TE,EE+lowE data [3].

### B. GW standard sirens

In this work, our analysis is based on the inspiral-only GW waveform. For the non-spinning inspiral of a

compact binary system, the GW waveform in frequency-domain is given by

$$\tilde{h}(f) = \frac{1}{D_{\text{eff}}} \sqrt{\frac{5}{24}} \frac{(G\mathcal{M}_{\text{chirp}})^{5/6}}{\pi^{2/3} c^{3/2}} f^{-7/6} \exp(-i\Psi). \quad (6)$$

The effective luminosity distance  $D_{\text{eff}}$  is defined as

$$D_{\text{eff}} = d_L \left[ F_+^2 \left( \frac{1 + \cos^2 \iota}{2} \right)^2 + F_\times^2 \cos^2 \iota \right]^{-1/2}, \quad (7)$$

where  $d_L$  is the luminosity distance to the GW source,  $\iota$  is the inclination angle between the orbital angular momentum axis of the binary and the line of sight,  $G$  is the gravitational constant,  $\mathcal{M}_{\text{chirp}} = M\eta^{3/5}(1+z)$  is the observed chirp mass,  $M = m_1 + m_2$  is the total mass of the binary system with component masses  $m_1$  and  $m_2$ , and  $\eta = m_1 m_2 / (m_1 + m_2)^2$  is the symmetric mass ratio. The GW phase  $\Psi$  is written to the second post-Newtonian order, which is related to the coalescence time  $t_c$  and the coalescence phase  $\psi_c$ . The detailed form of  $\Psi$  can be found in e.g., Ref. [126]. Here,  $F_{+,\times}$  are the antenna response functions, which are related to the location of the GW source ( $\theta, \phi$ ) and the polarization angle  $\psi$ . Since the space-based GW observatory could be viewed as two independent interferometers, the  $F_{+,\times}$  forms of the second independent interferometer are  $F_{+,\times}^{(2)}(t; \theta, \phi, \psi) = F_{+,\times}^{(1)}(t; \theta, \phi - \pi/4, \psi)$ . By adopting the low-frequency approximation, the forms of  $F_{+,\times}$  for Taiji are from Ref. [127], for TianQin are from Ref. [130], and for LISA are from Ref. [131]. To describe the GW signal in the Fourier space, the observation time  $t$  is replaced with  $t(f) = t_c - \frac{5}{256} \mathcal{M}_{\text{chirp}}^{-5/3} (\pi f)^{-8/3}$  [132, 133]. Here we consider Taiji in a heliocentric orbit ahead of the Earth by  $20^\circ$ , TianQin in a heliocentric orbit around the Earth, and LISA in a heliocentric orbit behind the Earth by  $20^\circ$ .

### C. Parameter estimation of MBHBs

The combined SNR for the detection network of  $N$  independent detectors is given by

$$\rho = (\tilde{\mathbf{h}} | \tilde{\mathbf{h}})^{1/2}, \quad (8)$$

where  $\tilde{\mathbf{h}}$  is the frequency domain GW waveform considering the detector network including  $N$  independent detectors and can be written as  $\tilde{\mathbf{h}} = [\tilde{h}_1, \tilde{h}_2, \dots, \tilde{h}_k, \dots, \tilde{h}_N]$ . Here  $\tilde{h}_k$  is the frequency domain GW waveform of the  $k$ -th detector. The inner product is defined as

$$(\tilde{\mathbf{h}} | \tilde{\mathbf{h}}) = \sum_{k=1}^N (\tilde{h}_k | \tilde{h}_k) = \sum_{k=1}^N 4 \int_{f_{\text{lower}}}^{f_{\text{upper}}} \frac{\tilde{h}_k(f) \tilde{h}_k^*(f)}{S_{n,k}(f)} df, \quad (9)$$

where  $*$  denotes the complex conjugate,  $f_{\text{lower}}$  is the lower frequency cutoff,  $f_{\text{upper}}$  is the upper limit (see Sec. III A

for more details), and  $S_{n,k}(f)$  is the sensitivity curve functions of the  $k$ -th detector when the low-frequency approximation [104, 131] is adopted for the response functions  $F_{+,\times}$ . We adopt the forms of  $S_n(f)$  for Taiji from Ref. [101], for TianQin from Ref. [105], and for LISA from Ref. [134], as shown in Fig. 1. The SNR threshold is set to be 8 in the simulation.

For a detector network, the Fisher information matrix can be written as

$$F_{ij} = \left( \frac{\partial \tilde{\mathbf{h}}}{\partial \theta_i} \middle| \frac{\partial \tilde{\mathbf{h}}}{\partial \theta_j} \right) = \sum_{k=1}^N \left( \frac{\partial \tilde{h}_k}{\partial \theta_i} \middle| \frac{\partial \tilde{h}_k}{\partial \theta_j} \right), \quad (10)$$

where  $\boldsymbol{\theta}$  denotes nine parameters ( $d_L, \mathcal{M}_{\text{chirp}}, \eta, \theta, \phi, \iota, t_c, \psi_c, \psi$ ) for a GW event. The covariance matrix is equal to the inverse of the Fisher matrix, i.e.,  $\text{Cov}_{ij} = (F^{-1})_{ij}$ . Thus the measurement error of GW parameter  $\theta_i$  is  $\Delta\theta_i = \sqrt{\text{Cov}_{ii}}$ . The sky localization error is given by

$$\Delta\Omega = 2\pi |\sin\theta| \sqrt{(\Delta\theta)^2 (\Delta\phi)^2 - (\Delta\theta\Delta\phi)^2}, \quad (11)$$

where  $\Delta\theta$ ,  $\Delta\phi$ , and  $\Delta\theta\Delta\phi$  are given by the covariance matrix.

If the GW signal is weakly lensed or the peculiar velocity of its host galaxy is not properly accounted for, the estimated luminosity distance is in error. Hence, in addition to the measurement error from GW observation, we also consider the errors from weak lensing and peculiar velocity. For the error caused by weak lensing, we adopt the fitting formula from Refs. [135, 136]

$$\sigma_{d_L}^{\text{lens}}(z) = d_L(z) \times 0.066 \left[ \frac{1 - (1+z)^{-0.25}}{0.25} \right]^{1.8}. \quad (12)$$

The error caused by the peculiar velocity of the GW source is given by [137]

$$\sigma_{d_L}^{\text{pv}}(z) = d_L(z) \times \left[ 1 + \frac{c(1+z)^2}{H(z)d_L(z)} \right] \frac{\sqrt{\langle v^2 \rangle}}{c}, \quad (13)$$

where  $H(z)$  is the Hubble parameter and  $\sqrt{\langle v^2 \rangle}$  is the peculiar velocity of the GW source. In this work, we set  $\sqrt{\langle v^2 \rangle} = 500 \text{ km} \cdot \text{s}^{-1}$ , in agreement with the average value observed in galaxy catalogs [66]. Hence, the total error of  $d_L$  is written as

$$\sigma_{d_L} = \sqrt{(\sigma_{d_L}^{\text{inst}})^2 + (\sigma_{d_L}^{\text{lens}})^2 + (\sigma_{d_L}^{\text{pv}})^2}. \quad (14)$$

For the bright sirens, we also need to additionally consider the errors caused by the redshift measurements  $\sigma_{d_L}^z$ . We make the assumption that redshift measurements at  $z < 2$  are determined spectroscopically with negligible errors. However, for the GW events with  $z > 2$  associated with photometric measurements [138, 139], the redshift errors are estimated as  $\Delta z \approx 0.03(1+z)$  [139, 140]. Following Refs. [73, 136, 138], we propagate the redshift errors to the distance errors by assuming our fiducial cosmology, i.e.,  $\sigma_{d_L}^z = \frac{\partial d_L}{\partial z} \Delta z$ .

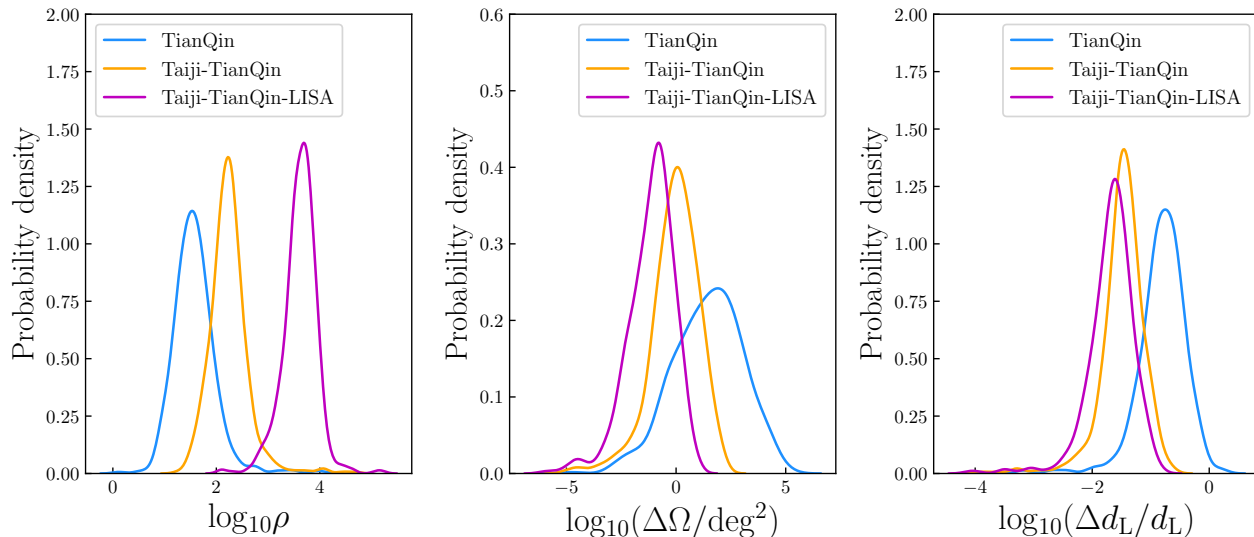


FIG. 2: Distributions of  $\rho$ ,  $\Delta\Omega$ , and  $\Delta d_L/d_L$  of 500 simulated MBHBs ( $z < 6$ ) for TianQin, Taiji-TianQin, and Taiji-TianQin-LISA based on the pop III model. Left panel: SNR distributions of TianQin, the Taiji-TianQin network, and the Taiji-TianQin-LISA network. Middle panel: sky localization error distributions of TianQin, the Taiji-TianQin network, and the Taiji-TianQin-LISA network. Right panel: relative uncertainty on luminosity distance distributions of TianQin, the Taiji-TianQin network, and the Taiji-TianQin-LISA network.

#### D. Galaxy localization

We first obtain the localization errors and luminosity distance errors of MBHBs. Meanwhile, we simulate the galaxy catalogs uniformly in a co-moving volume with a number density of  $0.02 \text{ Mpc}^{-3}$  [141] in the range of  $z \in [0, 3]$  (the adopted galaxy number density is in the middle of the observational error bars; see Fig. 1 of Ref. [141]). By combining the flat priors for  $\Omega_m \in [0.1, 0.5]$  and  $H_0 \in [60, 80]$ , and the luminosity distance errors, we obtain the lower and upper limits of redshift ( $z_{\min}$ ,  $z_{\max}$ ), assuming the  $\Lambda$ CDM model. We then derive the  $2 \times 2$  covariance matrix  $\text{Cov}[\theta, \phi]$  from the whole covariance matrix and use the new covariance matrix to calculate  $\chi^2$ , which describes the angular deviation from an arbitrary galaxy to the GW source and is given by

$$\chi^2 = \boldsymbol{\xi} (\text{Cov}^{-1}) \boldsymbol{\xi}^\top = \sum_{i,j} \xi_i (\text{Cov}^{-1})_{ij} \xi_j, \quad (15)$$

with  $\boldsymbol{\xi} = (\theta - \bar{\theta}, \phi - \bar{\phi})$ . Here  $(\bar{\theta}, \bar{\phi})$  represent the angular location of the GW source and  $(\theta, \phi)$  represent the angular location of an arbitrary galaxy. We adopt the boundary of the GW source's angular localization with  $\chi^2 = 9.21$ , corresponding to the 99% confidence level. Therefore, if the galaxies satisfy  $\chi^2 \leq 9.21$  and  $z \in [z_{\min}, z_{\max}]$ , they can be considered as the potential host galaxies of the GW source.

### III. SIMULATIONS

#### A. Simulations of GW catalogs

In this subsection, we detailedly introduce the simulations of MBHB catalogs. Following Refs. [73, 136, 142], we consider both the “light-seed” and “heavy-seed” scenarios for the seeding models of MBHB [141, 143, 144]. First, we would briefly introduce the seeding models of MBHB considered in this work.

(i) Model pop III: a light-seed scenario that assumes the MBH seed is the remnants of the first generation or population III stars, with a mass of around  $100 M_\odot$  [143, 145].

(ii) Model Q3d: a heavy-seed scenario that assumes the MBH seed is from the collapse of protogalactic disks [142], with a mass of  $\sim 10^5 M_\odot$ , and also considers the time delay between the merger of MBHBs and merger of galaxies.

(iii) Model Q3nod: same as Q3d, but not consider the time delay.

According to the merger rates of MBHBs predicted in Ref. [142], for the simulation of bright sirens, we simulated 877, 41, and 610 GW catalogs based on the pop III, Q3d, and Q3nod models. For the simulation of dark sirens, following Ref. [129], we make a reasonable assumption that it is difficult to obtain complete galaxy catalogs at  $z > 3$ , so we only select the GW events at  $z < 3$  for the three models of MBHB as the dark siren events and simulate the galaxy catalogs at  $z < 3$ . The number of the simulated dark siren data at  $z < 3$  are shown in Table III.

In this work, we consider the following observation

strategies for space-based GW detectors:

- **Taiji**: a space-based GW observatory consists of three satellites forming a triangle with the arm length of  $3 \times 10^6$  km, and the mission time is 5 years [101–103].
- **TianQin**: a space-based GW observatory consists of two constellations, each consisting of an equilateral triangle of three satellites with the arm length of  $\sqrt{3} \times 10^5$  km [104–109], and the mission time is 5 years.
- **LISA**: a space-based GW observatory consists of three satellites forming a triangle with the arm length of  $2.5 \times 10^6$  km [110–112], and the mission time is 5 years<sup>1</sup>.
- **Taiji+TianQin**: Taiji and TianQin observe together, with 5 years of overlap in operation time.
- **Taiji+TianQin+LISA**: Taiji, TianQin, and LISA observe together, with 5 years of overlap in operation time<sup>2</sup>.

The sky location  $(\theta, \phi)$ , the binary inclination angle  $\iota$ , the polarization angle  $\psi$ , the coalescence time  $t_c$ , and the coalescence phase  $\psi_c$  are randomly sampled in the ranges of  $\cos \theta \in [-1, 1]$ ,  $\phi \in [0, 2\pi]$ ,  $\cos \iota \in [-1, 1]$ ,  $\psi \in [0, 2\pi]$ ,  $t_c \in [0, 5]$  years, and  $\psi_c \in [0, 2\pi]$ , respectively. For the redshift and mass distributions of the three models, we use the numerical fitting formulas in Ref. [73] to fit the curves shown in Fig. 3 of Ref. [142]. For Taiji, TianQin, and LISA, we adopt the frequency in the range of  $[10^{-4}, 1]$  Hz. In the calculations of Eqs. (8) and (10),  $f_{\text{lower}}$  is chosen as  $f_{\text{lower}} = \max(f_{\text{obs}}, 10^{-4})$  Hz and  $f_{\text{upper}}$  is chosen as  $f_{\text{upper}} = \min(f_{\text{ISCO}}, 1)$  Hz. Here  $f_{\text{obs}} = (t_c/5)^{-3/8} \mathcal{M}_{\text{chirp}}^{-5/8} / 8\pi$  is the observation frequency at the coalescence time  $t_c$  and  $f_{\text{ISCO}}$  is the innermost stable circular orbit (ISCO) frequency  $f_{\text{upper}} = c^3/6\sqrt{6}\pi GM_{\text{obs}}$  with  $M_{\text{obs}} = (m_1 + m_2)(1 + z)$  [130].

## B. Bright sirens: observations of EM counterparts

Several works suggest that the mergers of MBHBs could emit EM radiations in the radio/optical band [113–

<sup>1</sup> In fact, the lifetime of LISA is commonly considered to be 4 years. However, LISA is also prepared to extend to 10 years [111]. Furthermore, recent work has shown that extending the mission to 6 years would greatly benefit scientific investigations [146].

<sup>2</sup> We assume that the duty cycle during the operation time is 100%, which means that the space-based GW detectors are continuously observing in the operation time. However, recent work shows that the duty cycle of LISA is only about 0.75 [146]. This indicates that it may take about 6.7 years of observation time to achieve the results in our analysis. Nonetheless, since Taiji, TianQin, and LISA all have the potential to extend their observation time, we consider this assumption to be reasonable.

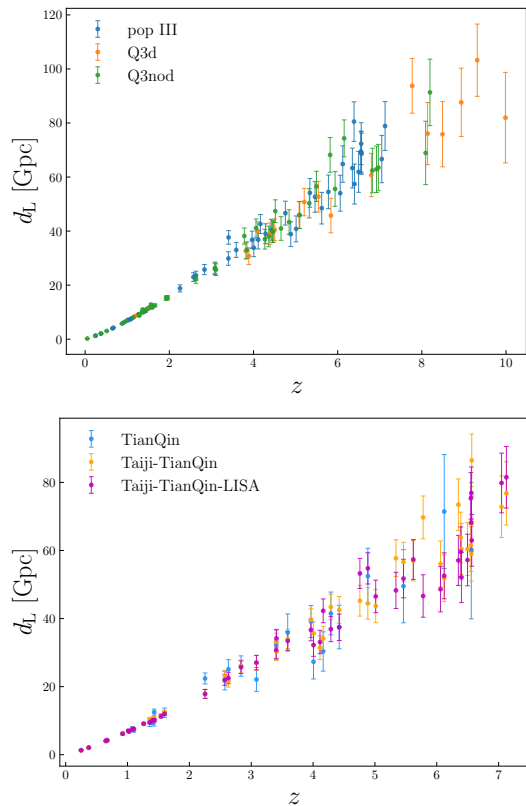


FIG. 3: The simulated bright siren data. Upper panel: the simulated bright sirens from the 5-year observation of the Taiji-TianQin-LISA network based on the pop III, Q3d, and Q3nod models. Lower panel: the simulated bright sirens from the 5-year observation of TianQin, the Taiji-TianQin network, and the Taiji-TianQin-LISA network based on the pop III model.

[120] (see Refs. [147, 148] for models which can emit EM radiations continuously in the inspiral phase). Redshift measurements are crucial for using MBHBs as standard sirens. To detect EM radiations from MBHBs, radio and optical telescopes must be aimed at the GW sources in advance. A conservative method is to select GW events with  $\rho \geq 8$  and  $\Delta\Omega \leq 10 \text{ deg}^2$  (corresponding to the field of view of LSST) during the inspiral-only phases of MBHBs as potential candidates for EM counterpart detections<sup>3</sup>. If the GW source can be located to better than  $10 \text{ deg}^2$ , it could provide early warning for radio/optical telescopes, such as SKA and ELT, thus greatly enhancing the detection of EM counterparts (see Appendix A for more details about the warning time).

In Fig. 2, we present the distributions of  $\rho$ ,  $\Delta\Omega$ , and

<sup>3</sup> We assume that real-time data analysis of the GW source position during the inspiral phase is feasible in the era of space-based GW observatories, thanks to the potential of deep learning algorithms [149–151].

TABLE I: The estimated detection rates of GW-EM events from TianQin, the Taiji-TianQin network, and the Taiji-TianQin-LISA network within 5-year operation time based on the pop III, Q3d, and Q3nod models.

Detection strategy	pop III		Q3d		Q3nod	
	Detection percentage	Number	Detection percentage	Number	Detection percentage	Number
TianQin	3.2%	28	24.3%	8	2.1%	13
Taiji-TianQin	5.6%	49	39%	16	5.9%	36
Taiji-TianQin-LISA	5.6%	49	44%	18	7%	43

$\Delta d_L/d_L$  for TianQin, Taiji-TianQin, and Taiji-TianQin-LISA based on the pop III model. These distributions are calculated by 500 random simulations in the redshift range of [0, 6]. We can see that the SNRs of Taiji-TianQin-LISA are the highest, followed by Taiji-TianQin and TianQin. For the sky localization errors, compared to the single TianQin observatory, the Taiji-TianQin network could greatly reduce sky localization errors. With the addition of the LISA observatory, the localization ability could be improved to a certain extent. For the measurement precisions of  $d_L$ , the above results still hold.

Previous work has shown that the EM counterparts detected by LSST are also detectable for SKA+ELT [136]. Therefore, we consider the strategy of SKA+ELT to observe EM counterparts in the radio and optical bands. We assume that the characterization of EM emission consists of radio flares and jets, and optical luminosity flares. In this case, the EM counterparts may first be detected by SKA in the radio band, and the host galaxies are then identified through localization. Then, the redshifts are determined spectroscopically or photometrically by the optical telescope ELT. The total luminosity in the radio band is given by  $L_{\text{radio}} = L_{\text{flare}} + L_{\text{jet}}$  (detailed forms of  $L_{\text{flare}}$  and  $L_{\text{jet}}$  can refer to Refs. [113–117, 136]). The luminosity that can be detected by SKA needs to satisfy the following relationship

$$\left(\frac{L_{\text{radio}}}{\text{erg/s}}\right) \left(\frac{d_L}{\text{cm}}\right)^{-2} \geq 4\pi 10^{-18} \left(\frac{F_{\nu, \text{min}}^{\text{SKA}}}{\mu\text{Jy}}\right) \left(\frac{\nu_{\text{SKA}}}{\text{GHz}}\right), \quad (16)$$

where  $F_{\text{min}}^{\text{SKA}}$  is the flux limit of SKA. Following Ref. [114], we assume that the bulk of the emission takes place in the SKA band, the form of  $F_{\text{min}}^{\text{SKA}}$  is  $F_{\text{min}}^{\text{SKA}} = \nu_{\text{SKA}} F_{\nu, \text{min}}^{\text{SKA}}$ , where  $\nu_{\text{SKA}} \simeq 1.4$  GHz and  $F_{\nu, \text{min}}^{\text{SKA}} \simeq 1$   $\mu\text{Jy}^4$ . Eq. (16) assumes that radio waves are emitted isotropically. Actually, the situation is not so straightforward, as the

synchrotron emission resulting from particle acceleration within the jet should be collimated along the jet direction. The jet's opening angle can cause a decrease in luminosity. However, if the jet is aligned towards us, we would receive a signal with a greater flux, which can lead to the detection of a dimmer source that would be otherwise undetectable. Since the two factors have opposite effects on the number of the GW-EM events and may counteract each other. Therefore, we adopt a simple approximation to treat the radio flux isotropically, which is also adopted in Refs. [73, 136].

The redshift information cannot be obtained from the identification of radio emission. Therefore, follow-up observations using ELT are required to search for EM emissions in the optical band and to determine the redshift. If the EM radiation in the optical band produced by the merger of MBHB satisfies the following expression, the redshift can be measured by ELT

$$m_{\text{gal}} = 82.5 - \frac{5}{2} \log_{10} \left( \frac{L_k \text{ s}}{3.02 \text{ erg}} \right) + 5 \log_{10} \left( \frac{d_L}{\text{pc}} \right) \leq m_{\text{ELT}}, \quad (17)$$

where  $m_{\text{gal}}$  is the apparent magnitude which is calculated by the host galaxy luminosity and  $L_k$  is the galaxy luminosity in the  $K$ -band. Here we follow Refs. [73, 136] and assume a fiducial mass-to-light ratio  $M/L_k = 0.03$  in the simulation (in fact,  $M/L_k$  for young stellar populations at moderate redshift is in the range of 0.01–0.05 [153]).  $m_{\text{ELT}} = 31.3$  is the detection threshold of ELT, which is the photometric limiting magnitude of ELT corresponding to the  $J$ -band and  $H$ -band. In principle, the threshold should be set to 30.2 corresponding to the  $K$ -band [154], because the apparent magnitude is calculated by the host galaxy's luminosity in  $K$ -band. Since MICADO (Multi-AO Imaging Camera for Deep Observations) on ELT will cover the range of 1000–2400 nm ( $J$ -band to  $K$ -band), we simply set the highest limiting magnitude as the threshold. Although this approach may slightly overestimate the detection threshold, it does not significantly affect the number of simulated bright sirens. In Refs. [125, 138], the authors adopt a simple method of taking into account the redshift error for all the GW events at  $z > 2$ , because the spectroscopic redshift at  $z > 2$  is usually unavailable [138, 139]. In fact,

<sup>4</sup> The current goal of SKA phase 1 mid-frequency is a flux limit of  $F_{\nu, \text{min}}^{\text{SKA}} \simeq 2$   $\mu\text{Jy}$  on a 0.5 deg<sup>2</sup> field of view assuming the integration time of 10 minutes (Table 1 of Ref. [152]). Considering the high performance of full SKA, we therefore assume that  $F_{\nu, \text{min}}^{\text{SKA}} \simeq 1$   $\mu\text{Jy}$  on approximately 10 deg<sup>2</sup>, in the same integration time [136].

as shown in Fig. 3, most simulated GW-EM events are at  $z > 2$ , i.e., the redshift errors are considered for most data points. On the other hand, the errors from lensing for the GW events at  $z > 2$  are dominant. Hence, such a treatment has only a minor impact on the cosmological parameter estimations.

The estimated detection rates of GW-EM events from TianQin, Taiji-TianQin, and Taiji-TianQin-LISA are shown in Table I. We can see that the number of detected GW-EM events from the Taiji-TianQin network almost double compared to the single TianQin observatory. For the heavy-seed models of MBHB, Q3d, and Q3nod, the addition of LISA could improve the number of detected GW-EM events. While for the light-seed model, pop III, the addition of LISA has no improvement for the number of detected GW-EM events. As shown in the middle panel of Fig. 2, the prime cause is that in the pop III model, the sky localization errors of the Taiji-TianQin network are good enough, and thus the addition of LISA could only improve the localization ability to some extent. For the Taiji-TianQin-LISA network, the detection rates of the pop III, Q3d, and Q3nod models are 5.6%, 44%, and 7%, respectively.

In Fig. 3, we show the simulated bright siren data. In the upper panel, we show the bright sirens from the Taiji-TianQin-LISA network based on the pop III, Q3d, and Q3nod models. We can see that for the Q3d model, the redshift of the bright sirens could reach  $z \sim 10$ . In the upper panel, we can see that the Taiji-TianQin-LISA network could detect the most number of bright sirens, followed by the Taiji-TianQin network and TianQin, also clearly shown in Table I. Moreover, the detector network could detect higher-redshift bright sirens than the single TianQin observatory.

We use the simulated bright siren data to perform cosmological analysis. We adopt the Markov Chain Monte Carlo (MCMC) method [155] to maximize the likelihood  $\mathcal{L}$  and infer the posterior probability distributions of cosmological parameters.

For the discussions about bright sirens, we adopt the pop III model of MBHB as the representative of the MBHB model. This is because (i) the pop III model typically offers intermediate constraints among the three models and (ii) the pop III model is less affected by the inspiral-merger-ringdown (IMR) waveform (while considering the IMR waveform has a significant correction for the heavy-seed model) [136], i.e., the number of GW-EM events based on the light-seed pop III model is less affected by the IMR waveform. Therefore, we use the pop III model to make discussions in the following.

We emphasize that our analysis is conservative because we adopt the GW waveform in the inspiral phase. As mentioned above, it is commonly believed that EM signals are emitted in the mergers of MBHBs. Hence, the warning time of EM counterparts is important for the application of the standard siren method (see Appendix A for more details). In addition, in order to obtain robust constraint results of cosmological parameters, we

randomly simulate 40 sets of bright siren data and adopt the data which give the medium constraint results as the final used bright siren data.

### C. Dark sirens: Bayesian method

For the GW events that the redshifts cannot be obtained by identifying EM counterparts, we need to use the cross-correlation of MBHBs and galaxy catalogs to obtain redshift information. In this subsection, we briefly introduce the method of using the dark siren method to infer the cosmological parameters. Using the method introduced in Sec. IID, we calculate the number of the potential host galaxies  $N_{\text{in}}$  and show the SNR- $N_{\text{in}}$  plot in Fig. 4.

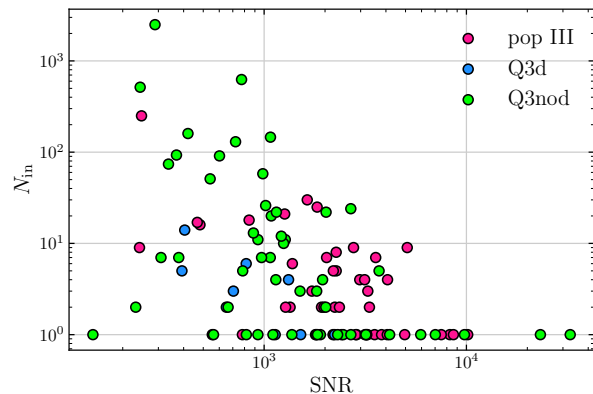


FIG. 4: Correlation between SNR of the dark siren from the Taiji-TianQin-LISA network and the number of the potential host galaxies  $N_{\text{in}}$  based on the pop III, Q3d, and Q3nod models.

We adopt the Bayesian method to infer the cosmological parameters, and the posterior probability distribution of the cosmological parameters  $\vec{\Omega}$  is

$$p(\vec{\Omega}|\vec{X}_{\text{GW}}, \vec{D}_{\text{GW}}) \propto p(\vec{\Omega})\mathcal{L}(\vec{X}_{\text{GW}}|\vec{D}_{\text{GW}}, \vec{\Omega}), \quad (18)$$

where  $\vec{X}_{\text{GW}}$  represent the GW data,  $\vec{D}_{\text{GW}}$  represent the detected GW events, and  $p(\vec{\Omega})$  are the prior distributions of the cosmological parameters. Assuming that the GW events are independent of each other, the likelihood of the GW data can be expressed as

$$\mathcal{L}(\vec{X}_{\text{GW}}|\vec{D}_{\text{GW}}, \vec{\Omega}) = \prod_{i=1}^{N_{\text{GW}}} \mathcal{L}(X_{\text{GW},i}|D_{\text{GW},i}, \vec{\Omega}), \quad (19)$$

where  $N_{\text{GW}}$  is the number of GW events. The likelihood function  $\mathcal{L}(X_{\text{GW}}|D_{\text{GW}}, \vec{\Omega})$  is obtained by marginalizing the redshifts of the GW events,

$$\mathcal{L}(X_{\text{GW}}|D_{\text{GW}}, \vec{\Omega}) = \frac{\int p(X_{\text{GW}}|d_L(z, \vec{\Omega}))p_z(z)dz}{\int p(D_{\text{GW}}|d_L(z, \vec{\Omega}))p_z(z)dz}, \quad (20)$$

where  $p(X_{\text{GW}}|d_L(z, \vec{\Omega}))$  is the probability of detecting the GW event at  $d_L(z, \vec{\Omega})$  and is given by

$$p(X_{\text{GW}}|d_L(z, \vec{\Omega})) = \frac{1}{\sqrt{2\pi}\sigma_{d_L}} \exp\left[-\frac{(\hat{d}_L - d_L(z, \vec{\Omega}))^2}{2\sigma_{d_L}^2}\right], \quad (21)$$

where  $\hat{d}_L$  is the observed luminosity distance of the GW source and the luminosity distance error  $\sigma_{d_L}$  can be obtained from Eq. (14).  $p_z(z)$  are the prior distributions of the redshifts of GW sources and can be expressed as,

$$p_z(z) \propto \frac{1}{N_{\text{in}}} \sum_{n=1}^{N_{\text{in}}} W_n \delta(\hat{z}_n - z), \quad (22)$$

where  $\delta(\hat{z}_n - z)$  is the delta function with  $\hat{z}_n$  being the redshift of the  $n$ -th potential host galaxy and  $W_n$  is the angular position weight of the  $n$ -th potential host galaxy

$$W_n \propto \exp\left(-\frac{1}{2}\chi_n^2\right). \quad (23)$$

Here  $\chi_n^2$  is obtained from Eq. (15).

Following Ref. [36], the GW selection effect is written as

$$\begin{aligned} p(D_{\text{GW}}|d_L(z, \vec{\Omega})) &= \int p(D_{\text{GW}}|d_L(z, \vec{\Omega}), X_{\text{GW}}) dX_{\text{GW}} \\ &= \frac{1}{N_{\text{sample}}} \sum_{i=1}^{N_{\text{sample}}} p(D_{\text{GW},i}|d_L(z, \vec{\Omega}), X_{\text{GW},i}), \end{aligned} \quad (24)$$

where  $N_{\text{sample}}$  is set to 50000 and  $X_{\text{GW},i}$  represents the  $i$ -th GW event whose luminosity distance is  $d_L(z, \vec{\Omega})$  and the other GW source parameters are randomly chosen according to their prior distributions.  $p(D_{\text{GW},i}|d_L(z, \vec{\Omega}), X_{\text{GW},i})$  is expressed as

$$p(D_{\text{GW},i}|d_L(z, \vec{\Omega}), X_{\text{GW},i}) = \begin{cases} 1, & \text{if } \rho_i > \rho_{\text{th}}, \\ 0, & \text{otherwise.} \end{cases} \quad (25)$$

#### IV. COSMOLOGICAL PARAMETER ESTIMATION

In this section, we shall report the constraint results of the cosmological parameters. We consider the optimistic (bright sirens) and conservative (dark sirens) scenarios to make the cosmological analysis. For the optimistic case, we use the simulated bright siren data from the Taiji-TianQin-LISA network to constrain the  $\Lambda$ CDM,  $w$ CDM, and the  $w_0 w_a$ CDM models by performing the Markov-chain Monte Carlo analysis [155]. In order to show the ability of the Taiji-TianQin-LISA network to break cosmological parameter degeneracies, we also show the constraint results of CMB and CMB+Taiji-TianQin-LISA.

For the CMB data, we employ the ‘‘Planck distance priors’’ from the Planck 2018 observation [3, 156]. The  $1\sigma$  and  $2\sigma$  posterior distribution contours for the cosmological parameters of interest are shown in Figs. 5 and 6 and the  $1\sigma$  errors for the marginalized parameter constraints are summarized in Table II. We also calculate the constraint results of TianQin and the Taiji-TianQin network for comparison. Other constraint results are shown in Appendix B. We use  $\sigma(\xi)$  and  $\varepsilon(\xi)$  to represent the absolute and relative errors of parameter  $\xi$ , with  $\varepsilon(\xi)$  defined as  $\varepsilon(\xi) = \sigma(\xi)/\xi$ . Note that we adopt the pop III model as the representative of the MBHB model to show the ability of the Taiji-TianQin-LISA network to break cosmological parameter degeneracies, as discussed in Sec. III A. For the conservative case, we use the dark sirens from the Taiji-TianQin-LISA network to constrain the  $\Lambda$ CDM model. The constraint results are shown in Figs. 6–8 and summarized in Table III.

##### A. Bright sirens

In the left panel of Fig. 5, we show the constraint results in the  $\Omega_m - H_0$  plane for the  $\Lambda$ CDM model using the simulated standard sirens from the Taiji-TianQin-LISA network based on the three population models of MBHB. As can be seen, Q3d gives the worst constraint results due to the least number of standard sirens. The detection number of pop III is more than that of Q3nod. However, the pop III and Q3nod models give similar constraint results. The prime cause is that Q3nod has more lower-redshift data points ( $z < 2$ ), so Q3nod (43 data points) gives comparable constraint results with those of pop III (49 data points). In the right panel of Fig. 5, in order to clearly show the ability of the Taiji-TianQin-LISA network to constrain cosmological parameters, we show the constraints using the simulated standard siren data from TianQin, the Taiji-TianQin network, and the Taiji-TianQin-LISA network based on pop III. We could see that Taiji-TianQin-LISA gives the best constraints, followed by Taiji-TianQin and TianQin. Compared with TianQin, the Taiji-TianQin network could significantly improve the constraint precisions of cosmological parameters. With the addition of LISA to the Taiji-TianQin network, the constraint precisions of cosmological parameters are improved slightly. In the scenario of pop III, the Taiji-TianQin network gives  $\sigma(\Omega_m) = 0.019$  and  $\sigma(H_0) = 0.63 \text{ km s}^{-1} \text{ Mpc}^{-1}$ , which are 53.7% [(0.041-0.019)/0.041] and 42.7% [(1.10-0.63)/1.10] better than those of TianQin. In fact, the Taiji-TianQin network could constrain the Hubble constant to a precision of 0.9%. Meanwhile, the Taiji-TianQin-LISA network gives almost the same constraints on  $\Omega_m$  and  $H_0$ .

In Fig. 6, we show the constraints on the  $\Lambda$ CDM,  $w$ CDM, and  $w_0 w_a$ CDM models using the CMB, Taiji-TianQin-LISA (pop III), and the CMB+Taiji-TianQin-LISA (pop III) data. We first focus on the  $\Lambda$ CDM model. From Fig. 6(a), we can see that the contours of CMB and

TABLE II: The absolute errors ( $1\sigma$ ) and the relative errors of the cosmological parameters in the  $\Lambda$ CDM,  $w$ CDM, and  $w_0w_a$ CDM models using the CMB, Taiji-TianQin-LISA (pop III), and CMB+Taiji-TianQin-LISA (pop III) data. Here,  $H_0$  is in units of  $\text{km s}^{-1} \text{Mpc}^{-1}$ .

Error	$\Lambda$ CDM			$w$ CDM			$w_0w_a$ CDM		
	CMB	Taiji-TianQin-LISA	CMB+Taiji-TianQin-LISA	CMB	Taiji-TianQin-LISA	CMB+Taiji-TianQin-LISA	CMB	Taiji-TianQin-LISA	CMB+Taiji-TianQin-LISA
$\sigma(\Omega_m)$	0.009	0.019	0.005	0.064	0.027	0.007	0.060	0.056	0.017
$\sigma(H_0)$	0.61	0.62	0.38	7.30	1.40	0.71	6.10	2.00	1.70
$\sigma(w)$	–	–	–	0.250	0.200	0.036	–	–	–
$\sigma(w_0)$	–	–	–	–	–	–	0.610	0.330	0.230
$\sigma(w_a)$	–	–	–	–	–	–	–	1.70	0.63
$\varepsilon(\Omega_m)$	2.7%	5.8%	1.7%	20.5%	8.5%	2.0%	18.6%	15.5%	5.3%
$\varepsilon(H_0)$	0.9%	0.9%	0.6%	10.6%	2.1%	1.1%	9.0%	3.0%	2.5%
$\varepsilon(w)$	–	–	–	23.8%	18.9%	3.6%	–	–	–
$\varepsilon(w_0)$	–	–	–	–	–	–	98.3%	36.7%	23.4%

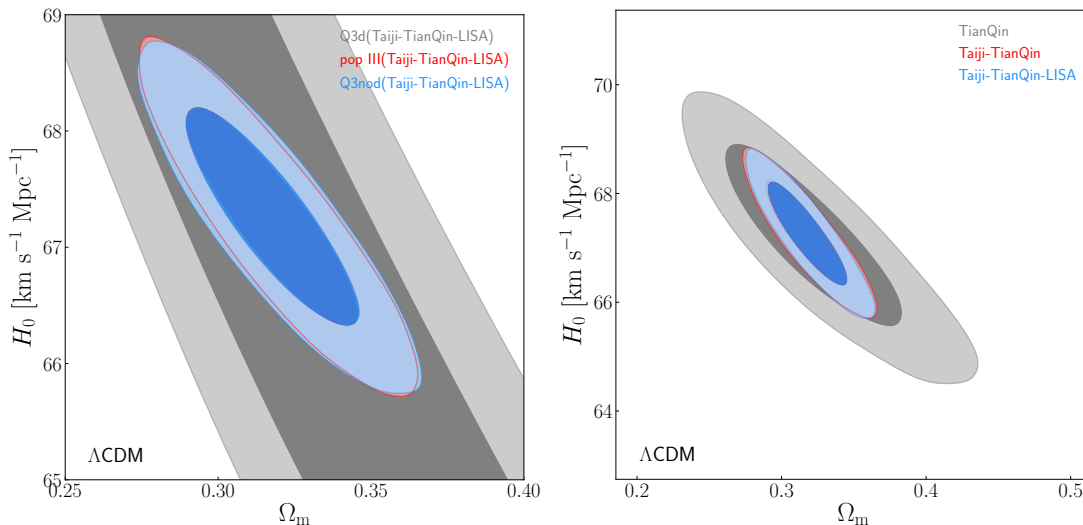


FIG. 5: Constraints on the  $\Lambda$ CDM model. Left panel: Two-dimensional marginalized contours (68.3% and 95.4% confidence level) in the  $\Omega_m$ - $H_0$  plane using the simulated bright siren data from the Taiji-TianQin-LISA network based on the pop III, Q3d, and Q3nod models. Right panel: Two-dimensional marginalized contours (68.3% and 95.4% confidence level) in the  $\Omega_m$ - $H_0$  plane using the simulated bright siren data from TianQin, the Taiji-TianQin network, and the Taiji-TianQin-LISA network based on the pop III model.

Taiji-TianQin-LISA show different orientations and thus the combination of them could break the parameter degeneracies. The combination of CMB and Taiji-TianQin-LISA gives  $\sigma(\Omega_m) = 0.005$  and  $\sigma(H_0) = 0.38 \text{ km s}^{-1} \text{Mpc}^{-1}$ , which are 44.4% and 37.7% better than those of CMB. In Figs. 6(b) and 6(c), we show the cases in the  $w$ CDM model. We can see that the contours of CMB and Taiji-TianQin-LISA also show different orientations. In particular, the parameter degeneracy orientations in the  $w$ - $\Omega_m$  are almost orthogonal. Hence, the combination of them could effectively break the cosmological parameter degeneracies and greatly improve the constraint precisions of cosmological parameters. The combination of CMB and Taiji-TianQin-LISA gives  $\sigma(\Omega_m) = 0.007$ ,  $\sigma(H_0) = 0.71 \text{ km s}^{-1} \text{Mpc}^{-1}$ , and  $\sigma(w) = 0.036$ , which are 89.1%, 90.3%, and 85.6% better than those of CMB. Moreover, the constraint precision of  $w$  is 3.6%, which is

close to the latest constraint results by the CMB+SN data [157]. In Fig. 6(d), we show the constraint results in the  $w_0w_a$ CDM model. Also, the combination of CMB and Taiji-TianQin-LISA could break cosmological parameter degeneracies. The combination of CMB and Taiji-TianQin-LISA gives  $\sigma(w_0) = 0.23$  which is 62.3% better than the constraint by the CMB data.

## B. Dark sirens

In Fig. 7, we show the constraints in the  $\Omega_m$ - $H_0$  plane for the pop III model. We can see that the Taiji-TianQin-LISA network gives  $\sigma(\Omega_m) = 0.0265$  and  $\sigma(H_0) = 0.765$ , which are all worse than the constraint results by the simulated bright sirens from the Taiji-TianQin-LISA network. However, the constraint precision of  $H_0$  is 1.13%,

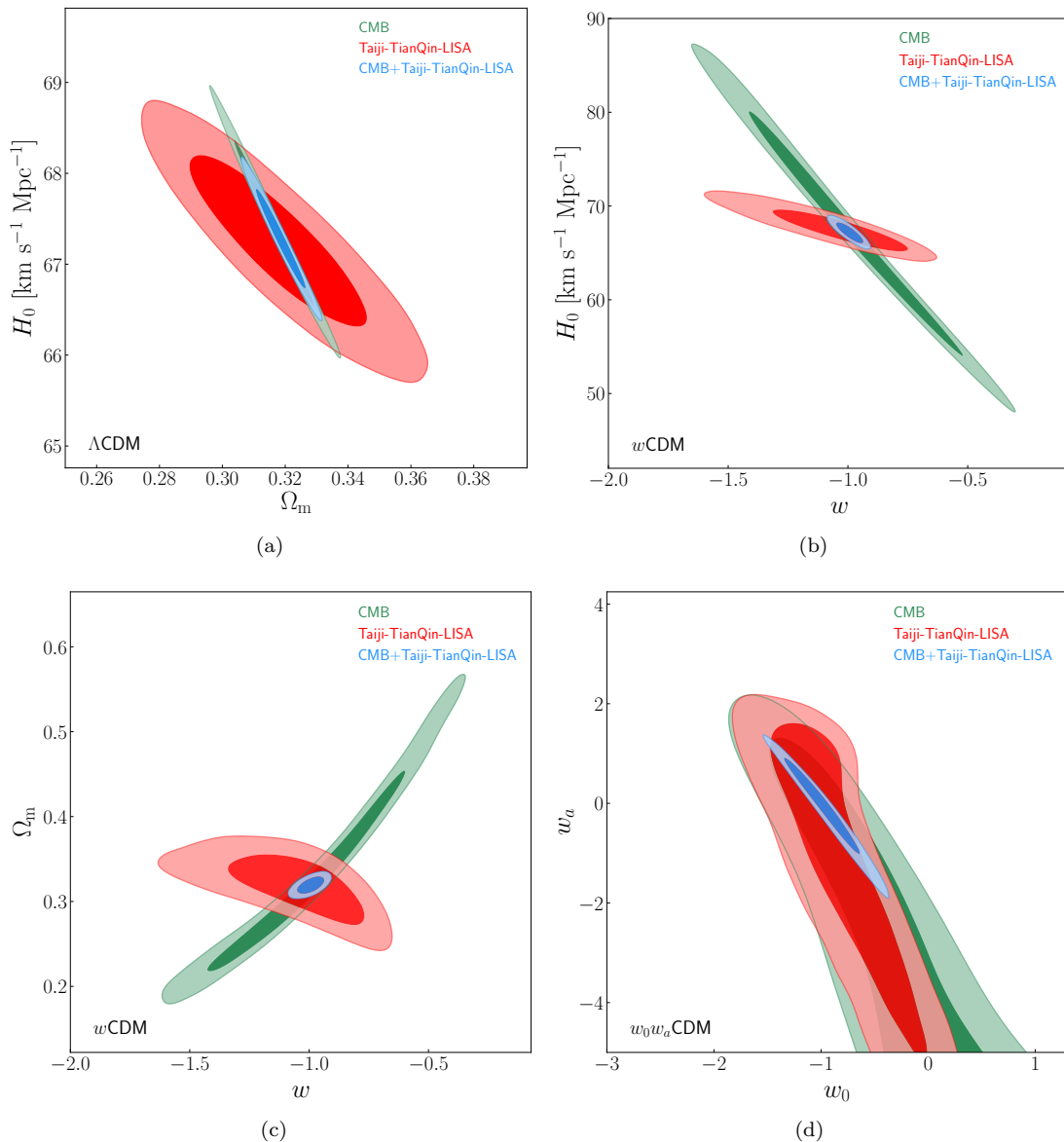


FIG. 6: Constraints on the  $\Lambda$ CDM,  $w$ CDM, and  $w_0 w_a$ CDM models using the CMB, Taiji-TianQin-LISA, and CMB+Taiji-TianQin-LISA data. Panel (a): Two-dimensional marginalized contours (68.3% and 95.4% confidence level) in the  $\Omega_m$ - $H_0$  plane for the  $\Lambda$ CDM model using the CMB, Taiji-TianQin-LISA, and CMB+Taiji-TianQin-LISA data. Panel (b): Similar to panel (a), but in the  $w$ - $H_0$  plane for the  $w$ CDM model. Panel (c): Similar to panel (a), but in the  $w$ - $\Omega_m$  plane for the  $w$ CDM model. Panel (d): Similar to panel (a), but in the  $w_0$ - $w_a$  plane for the  $w_0 w_a$ CDM model. The Taiji-TianQin-LISA data are simulated based on the pop III model.

rather close to the standard of precision cosmology. In Fig. 8, we show the case for the Q3d model. The Taiji-TianQin-LISA network gives poor constraints  $\sigma(\Omega_m) = 0.121$  and  $\sigma(H_0) = 6.025$  due to the low merger rate of MBHB. In Fig. 9, we show the case for the Q3nod model. In this case, the Taiji-TianQin-LISA network gives similar constraint results to those of the pop III model. The constraint precision of  $H_0$  is 1.10%, also almost meeting the standard of precision cosmology. Our results show that the dark sirens of the Taiji-TianQin-LISA could also

play a crucial role in helping solve the Hubble tension. It is worth expecting that the Hubble tension could be solved with the help of the Taiji-TianQin-LISA network.

## V. CONCLUSION

In this work, we show the potential of the future standard sirens from the Taiji-TianQin-LISA network in constraining cosmological parameters. We consider the op-

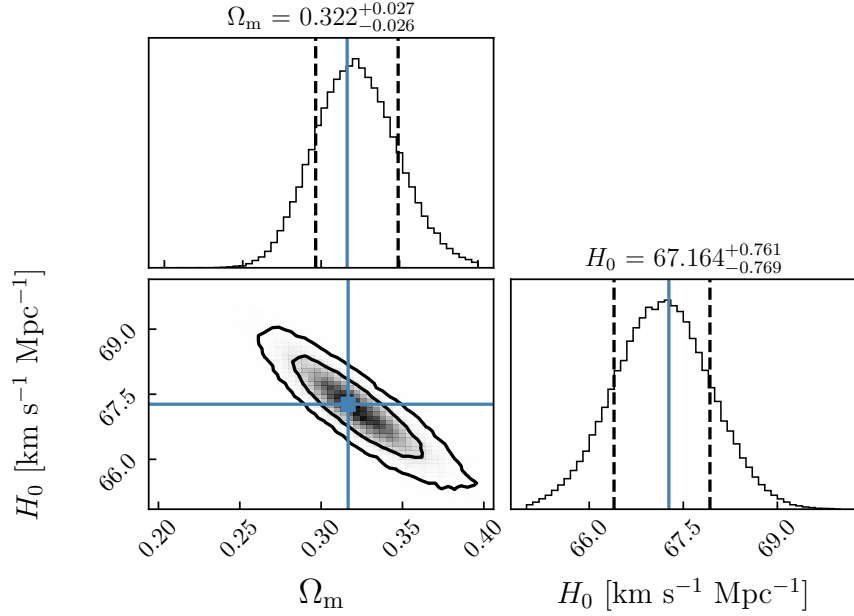


FIG. 7: Constraints on the  $\Lambda$ CDM model using the mock dark siren data from the Taiji-TianQin-LISA network based on the pop III model. Here the galaxy catalogs are uniformly simulated in a co-moving volume with a number density of  $0.02 \text{ Mpc}^{-3}$  [141] in the range of  $z \in [0, 3]$  as described in Sec. III D.

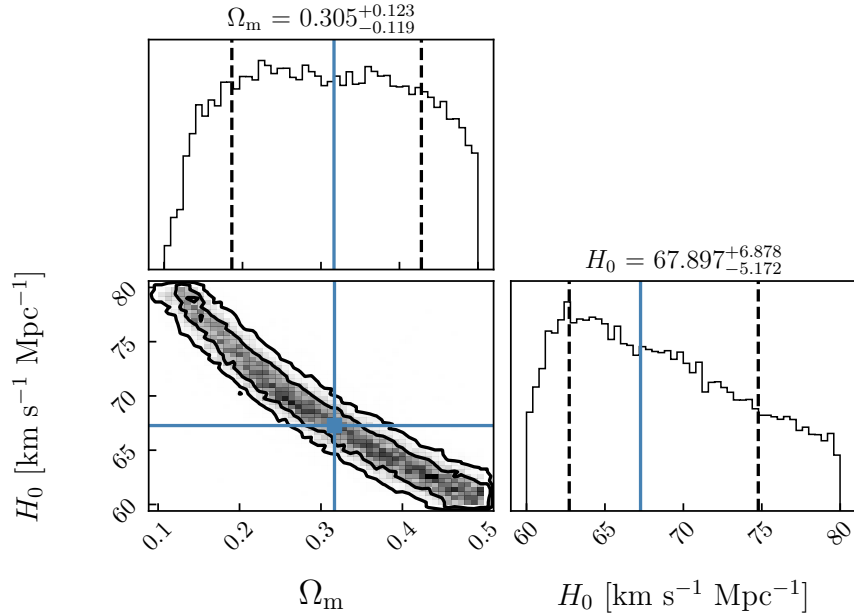


FIG. 8: Same as Fig. 7, but for the Q3d model.

timistic and conservative scenarios of the standard siren observations, i.e., the bright and dark sirens. Three population models of MBHB, i.e., pop III, Q3d, and Q3nod, are used to simulate the MBHB catalogs. For the simulations of bright sirens, we calculate the expected detection rates of the GW-EM events based on the three MBHB models. For comparison, we also show the results of the single TianQin observatory and the Taiji-TianQin net-

work. For the analysis of the simulated bright siren data on constraining cosmological parameters, we choose three typical cosmological models, i.e., the  $\Lambda$ CDM,  $w$ CDM, and  $w_0 w_a$ CDM models. In the dark siren case, we used the simulated GW events at  $z < 3$  combined with the simulated galaxy catalog to estimate cosmological parameters in the  $\Lambda$ CDM model.

We find that the bright siren data from the Taiji-

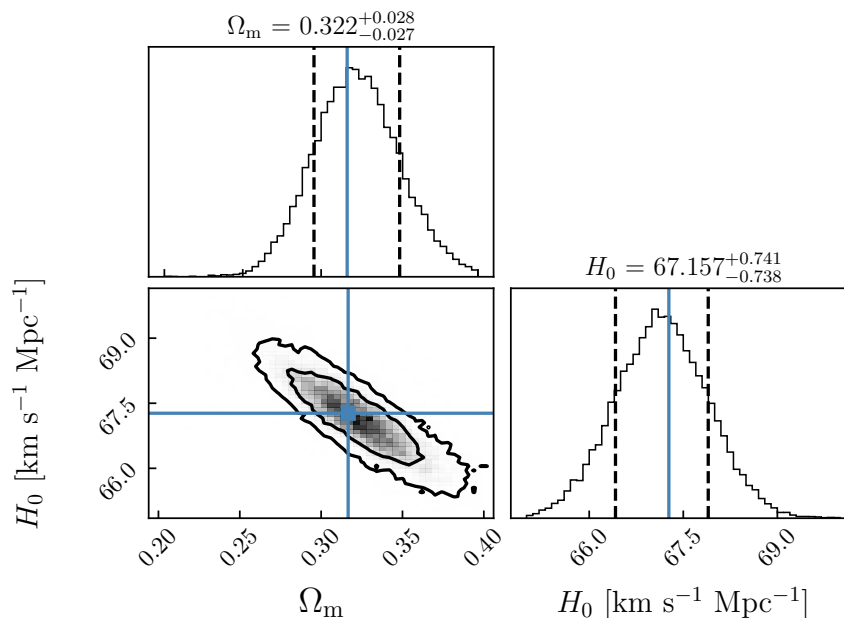


FIG. 9: Same as Fig. 7, but for the Q3nod model.

TABLE III: Constraint results of the dark sirens from the Taiji-TianQin-LISA network based on the pop III, Q3d, and Q3nod models. The first column represents the MBHB model, the second column represents the number of the simulated dark siren data at  $z < 3$  used in this work, the third to fifth columns represent the percentages of GW events with  $N_{\text{in}} = 1$ ,  $N_{\text{in}} \leq 10$ ,  $N_{\text{in}} \leq 100$ , and  $N_{\text{in}} \leq 1000$ , the sixth column represents the relative errors of  $\Omega_m$ , and the seventh column represents the relative errors of  $H_0$ .

MBHB model	Total number	$N_{\text{in}} = 1$	$N_{\text{in}} \leq 10$	$N_{\text{in}} \leq 100$	$\varepsilon(\Omega_m)$	$\varepsilon(H_0)$
pop III	46	40.4%	85.1%	97.9%	8.2%	1.13%
Q3d	8	33.3%	88.9%	100%	39.7%	8.87%
Q3nod	51	34.6%	61.5%	88.5%	8.5%	1.10%

TianQin-LISA network based on the pop III and Q3nod models could give tight constraints on the Hubble constant, with both constraint precisions being 0.9%. Nevertheless, the EoS parameters of dark energy could not be well constrained by the bright siren data from the Taiji-TianQin-LISA network (pop III and Q3nod). Fortunately, the Taiji-TianQin-LISA network and CMB show different parameter degeneracy orientations, especially in the dynamical dark energy models. Therefore, the combination of the Taiji-TianQin-LISA network and CMB could break cosmological parameter degeneracies and improve the constraint precisions of cosmological parameters. In addition, the Taiji-TianQin network gives comparable constraint results with those of the Taiji-TianQin-LISA network, which may indicate that the two space-based detector network is sufficient to constrain cosmological parameters well. Since the expected detection number of GW-EM events based on the Q3d model is small, Q3d gives loose constraints on all cosmological parameters. Concretely, the constraint pre-

cisions of  $\Omega_m$  and  $H_0$  using CMB+Taiji-TianQin-LISA (pop III) are 1.7% and 0.6%, which are close to or better than 1% (the standard of precision cosmology). While in the  $w$ CDM model, CMB+Taiji-TianQin-LISA (pop III) gives  $\sigma(w) = 0.036$ , which is 85.6% better than the constraint given by the CMB data. In the  $w_0 w_a$ CDM model, CMB+Taiji-TianQin-LISA (pop III) gives  $\sigma(w_0) = 0.23$  and  $\sigma(w_a) = 0.63$ . For the dark sirens from the Taiji-TianQin-LISA network, the constraint precisions of  $H_0$  based on the pop III, Q3d, and Q3nod models are 1.13%, 8.87%, and 1.10%, respectively, indicating that the dark sirens from the Taiji-TianQin-LISA network may also play a crucial role in measuring the Hubble constant.

Hence, we can conclude that: (i) the bright sirens from the Taiji-TianQin-LISA network could precisely measure the Hubble constant with a precision of 0.9%, but are poor at measuring dark energy; (ii) the bright sirens from the Taiji-TianQin-LISA network could effectively break the cosmological parameter degeneracies generated by the CMB data, especially in the dynamical dark en-

ergy models; (iii) the dark sirens from the Taiji-TianQin-LISA network could also provide a tight constraint on the Hubble constant, with a precision of 1.1%. It is worth expecting to use the Taiji-TianQin-LISA network to help solve the Hubble tension and explore the nature of dark energy.

### Acknowledgments

We thank Liang-Gui Zhu and Yue Shao for helpful discussions. This work was supported by the National SKA Program of China (Grants Nos. 2022SKA0110200 and 2022SKA0110203) and the National Natural Science Foundation of China (Grants Nos. 11975072, 11875102, and 11835009).

## Appendix

### Appendix A: Warning time of EM counterparts

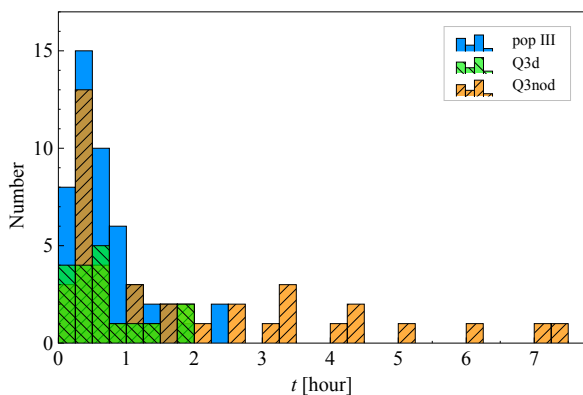


FIG. A10: The warning time distributions of the simulated bright sirens based on the pop III, Q3d, and Q3nod models.

In this Appendix, we provide more information about the detections of EM counterparts. In this work, we adopt the inspiral-only GW waveform and simulate the bright sirens. It is commonly believed that the EM radiations are emitted in the mergers of MBHBs. Hence, the warning times of EM counterparts are important for the detections of EM counterparts. The warning times of EM counterparts  $t_{\text{warning}}$  can be calculated by the integration upper limit  $f_{\text{upper}}$ . We have

$$t_{\text{warning}} = \frac{5\mathcal{M}_{\text{chirp}}}{(8\pi\mathcal{M}_{\text{chirp}}f)^{8/3}}. \quad (\text{A1})$$

Here we use  $f = f_{\text{upper}}$  to calculate the warning time. Note again that we assume the real-time data analysis of the GW source. In actual observation,  $f$  should be replaced by the frequency that meets  $\rho \geq 8$  and  $\Delta\Omega \leq 10 \text{ deg}^2$ . In our analysis, we consider that the warning could only be issued once  $f$  reaches  $f_{\text{upper}}$ . In Fig. A10, we show the warning time distributions of the simulated bright sirens based on the pop III, Q3d, and Q3nod models. We can see that the warning times are on the order of hours.

### Appendix B: Constraint results of cosmological parameters

- 
- [1] D. N. Spergel et al. (WMAP), *Astrophys. J. Suppl.* **148**, 175 (2003), astro-ph/0302209.
  - [2] C. L. Bennett et al. (WMAP), *Astrophys. J. Suppl.* **148**, 1 (2003), astro-ph/0302207.
  - [3] N. Aghanim et al. (Planck), *Astron. Astrophys.* **641**, A6 (2020), [Erratum: *Astron. Astrophys.* 652, C4 (2021)], 1807.06209.
  - [4] A. G. Riess et al., *Astrophys. J. Lett.* **934**, L7 (2022), 2112.04510.
  - [5] L. Verde, T. Treu, and A. G. Riess, *Nature Astron.* **3**, 891 (2019), 1907.10625.
  - [6] A. G. Riess, *Nature Rev. Phys.* **2**, 10 (2019), 2001.03624.
  - [7] M. Kamionkowski and A. G. Riess (2022), 2211.04492.
  - [8] R.-Y. Guo, J.-F. Zhang, and X. Zhang, *JCAP* **02**, 054 (2019), 1809.02340.
  - [9] L. Perivolaropoulos and F. Skara, *New Astron. Rev.* **95**, 101659 (2022), 2105.05208.
  - [10] L.-Y. Gao, Z.-W. Zhao, S.-S. Xue, and X. Zhang, *JCAP* **07**, 005 (2021), 2101.10714.
  - [11] E. Di Valentino, O. Mena, S. Pan, L. Visinelli, W. Yang, A. Melchiorri, D. F. Mota, A. G. Riess, and J. Silk, *Class. Quant. Grav.* **38**, 153001 (2021), 2103.01183.
  - [12] E. Abdalla et al., *JHEAp* **34**, 49 (2022), 2203.06142.
  - [13] R.-G. Cai, Z.-K. Guo, L. Li, S.-J. Wang, and W.-W. Yu, *Phys. Rev. D* **103**, 121302 (2021), 2102.02020.
  - [14] W. Yang, S. Pan, E. Di Valentino, R. C. Nunes, S. Vagnozzi, and D. F. Mota, *JCAP* **09**, 019 (2018), 1805.08252.
  - [15] E. Di Valentino et al., *Astropart. Phys.* **131**, 102605 (2021), 2008.11284.
  - [16] E. Di Valentino, A. Melchiorri, O. Mena, and S. Vagnozzi, *Phys. Dark Univ.* **30**, 100666 (2020),

TABLE B4: The absolute errors ( $1\sigma$ ) and the relative errors of the cosmological parameters in the  $\Lambda$ CDM,  $w$ CDM, and  $w_0w_a$ CDM models using the simulated bright siren data from TianQin, the Taiji-TianQin network, and the Taiji-TianQin-LISA network based on the pop III, Q3d, and Q3nod models. Note that  $H_0$  is in units of  $\text{km s}^{-1} \text{Mpc}^{-1}$ .

Model	Detection strategy	MBHB model	$\sigma(\Omega_m)$	$\sigma(H_0)$	$\sigma(w)$	$\sigma(w_0)$	$\sigma(w_a)$	$\varepsilon(\Omega_m)$	$\varepsilon(H_0)$	$\varepsilon(w)$	$\varepsilon(w_0)$
$\Lambda$ CDM	TianQin	pop III	0.041	1.10	–	–	–	12.5%	1.6%	–	–
		Q3d	0.245	9.95	–	–	–	52.1%	15.7%	–	–
		Q3nod	0.057	1.20	–	–	–	17.1%	1.8%	–	–
	Taiji-TianQin	pop III	0.019	0.63	–	–	–	6.0%	0.9%	–	–
		Q3d	0.106	5.60	–	–	–	28.4%	8.5%	–	–
		Q3nod	0.021	0.64	–	–	–	6.6%	1.0%	–	–
	Taiji-TianQin-LISA	pop III	0.019	0.63	–	–	–	5.8%	0.9%	–	–
		Q3d	0.096	5.15	–	–	–	26.1%	7.9%	–	–
		Q3nod	0.019	0.62	–	–	–	5.8%	0.9%	–	–
$w$ CDM	TianQin	pop III	0.057	2.60	0.395	–	–	17.8%	3.8%	35.0%	–
		Q3d	0.275	9.90	0.695	–	–	56.1%	16.3%	73.9%	–
		Q3nod	0.077	2.90	0.520	–	–	24.7%	4.3%	44.8%	–
	Taiji-TianQin	pop III	0.026	1.50	0.195	–	–	8.0%	2.2%	18.4%	–
		Q3d	0.116	9.95	0.650	–	–	34.2%	14.9%	62.5%	–
		Q3nod	0.030	1.45	0.205	–	–	9.2%	2.1%	19.3%	–
	Taiji-TianQin-LISA	pop III	0.026	1.45	0.190	–	–	8.0%	2.1%	17.9%	–
		Q3d	0.105	9.80	0.630	–	–	32.0%	14.7%	60.6%	–
		Q3nod	0.027	1.40	0.200	–	–	8.5%	2.1%	18.9%	–
$w_0w_a$ CDM	TianQin	pop III	0.063	4.15	–	0.680	2.30	18.4%	6.0%	–	57.6%
		Q3d	0.260	14.00	–	–	–	50.0%	22.6%	–	–
		Q3nod	0.081	5.30	–	–	–	24.0%	7.5%	–	–
	Taiji-TianQin	pop III	0.053	2.60	–	0.420	2.05	15.9%	3.9%	–	50.0%
		Q3d	0.150	10.00	–	1.130	–	38.9%	14.9%	–	–
		Q3nod	0.056	2.10	–	0.340	1.80	17.4%	3.1%	–	37.3%
	Taiji-TianQin-LISA	pop III	0.052	2.60	–	0.420	2.00	15.6%	3.9%	–	50.0%
		Q3d	0.140	10.00	–	1.120	–	37.8%	14.7%	–	–
		Q3nod	0.056	2.00	–	0.330	1.70	15.5%	3.0%	–	36.7%

1908.04281.

- [17] E. Di Valentino, A. Melchiorri, O. Mena, and S. Vagnozzi, *Phys. Rev. D* **101**, 063502 (2020), 1910.09853.
- [18] M. Liu, Z. Huang, X. Luo, H. Miao, N. K. Singh, and L. Huang, *Sci. China Phys. Mech. Astron.* **63**, 290405 (2020), 1912.00190.
- [19] X. Zhang and Q.-G. Huang, *Sci. China Phys. Mech. Astron.* **63**, 290402 (2020), 1911.09439.
- [20] Q. Ding, T. Nakama, and Y. Wang, *Sci. China Phys. Mech. Astron.* **63**, 290403 (2020), 1912.12600.
- [21] H. Li and X. Zhang, *Sci. Bull.* **65**, 1419 (2020), 2005.10458.
- [22] L.-F. Wang, J.-H. Zhang, D.-Z. He, J.-F. Zhang, and X. Zhang, *Mon. Not. Roy. Astron. Soc.* **514**, 1433 (2022), 2102.09331.
- [23] S. Vagnozzi, F. Pacucci, and A. Loeb, *JHEAp* **36**, 27 (2022), 2105.10421.
- [24] S. Vagnozzi, *Phys. Rev. D* **104**, 063524 (2021), 2105.10425.
- [25] S. Vagnozzi, *Phys. Rev. D* **102**, 023518 (2020), 1907.07569.
- [26] R.-Y. Guo, J.-F. Zhang, and X. Zhang, *Sci. China Phys. Mech. Astron.* **63**, 290406 (2020), 1910.13944.

- [27] L. Feng, D.-Z. He, H.-L. Li, J.-F. Zhang, and X. Zhang, *Sci. China Phys. Mech. Astron.* **63**, 290404 (2020), 1910.03872.
- [28] M.-X. Lin, W. Hu, and M. Raveri, *Phys. Rev. D* **102**, 123523 (2020), 2009.08974.
- [29] L.-Y. Gao, S.-S. Xue, and X. Zhang (2022), 2212.13146.
- [30] Z.-W. Zhao, J.-G. Zhang, Y. Li, J.-M. Zou, J.-F. Zhang, and X. Zhang (2022), 2212.13433.
- [31] B. F. Schutz, *Nature* **323**, 310 (1986).
- [32] D. E. Holz and S. A. Hughes, *Astrophys. J.* **629**, 15 (2005), astro-ph/0504616.
- [33] B. P. Abbott et al. (LIGO Scientific, Virgo, 1M2H, Dark Energy Camera GW-E, DES, DLT40, Las Cumbres Observatory, VINROUGE, MASTER), *Nature* **551**, 85 (2017), 1710.05835.
- [34] H.-Y. Chen, M. Fishbach, and D. E. Holz, *Nature* **562**, 545 (2018), 1712.06531.
- [35] N. Muttoni, D. Laghi, N. Tamanini, S. Marsat, and D. Izquierdo-Villalba (2023), 2303.10693.
- [36] R. Gray et al., *Phys. Rev. D* **101**, 122001 (2020), 1908.06050.
- [37] A. Finke, S. Foffa, F. Iacovelli, M. Maggiore, and M. Mancarella, *JCAP* **08**, 026 (2021), 2101.12660.
- [38] J. R. Gair et al. (2022), 2212.08694.
- [39] J.-Y. Song, L.-F. Wang, Y. Li, Z.-W. Zhao, J.-F. Zhang, W. Zhao, and X. Zhang (2022), 2212.00531.
- [40] H. Leandro, V. Marra, and R. Sturani, *Phys. Rev. D* **105**, 023523 (2022), 2109.07537.
- [41] W. Del Pozzo, *Phys. Rev. D* **86**, 043011 (2012), 1108.1317.
- [42] M. Fishbach et al. (LIGO Scientific, Virgo), *Astrophys. J. Lett.* **871**, L13 (2019), 1807.05667.
- [43] T. Yang, R.-G. Cai, and H. M. Lee, *JCAP* **10**, 061 (2022), 2208.10998.
- [44] M. Soares-Santos et al. (DES, LIGO Scientific, Virgo), *Astrophys. J. Lett.* **876**, L7 (2019), 1901.01540.
- [45] R. Nair, S. Bose, and T. D. Saini, *Phys. Rev. D* **98**, 023502 (2018), 1804.06085.
- [46] A. Palmese et al. (DES), *Astrophys. J. Lett.* **900**, L33 (2020), 2006.14961.
- [47] B. P. Abbott et al. (LIGO Scientific, Virgo, VIRGO), *Astrophys. J.* **909**, 218 (2021), [Erratum: *Astrophys. J.* 923, 279 (2021)], 1908.06060.
- [48] J. Yu, Y. Wang, W. Zhao, and Y. Lu, *Mon. Not. Roy. Astron. Soc.* **498**, 1786 (2020), 2003.06586.
- [49] R. Abbott et al. (LIGO Scientific, VIRGO, KAGRA) (2021), 2111.03604.
- [50] A. Palmese, C. R. Bom, S. Mucesh, and W. G. Hartley (2021), 2111.06445.
- [51] N. Dalal, D. E. Holz, S. A. Hughes, and B. Jain, *Phys. Rev. D* **74**, 063006 (2006), astro-ph/0601275.
- [52] C. Cutler and D. E. Holz, *Phys. Rev. D* **80**, 104009 (2009), 0906.3752.
- [53] S. Nissanke, D. E. Holz, S. A. Hughes, N. Dalal, and J. L. Sievers, *Astrophys. J.* **725**, 496 (2010), 0904.1017.
- [54] R.-G. Cai, Z. Cao, Z.-K. Guo, S.-J. Wang, and T. Yang, *Natl. Sci. Rev.* **4**, 687 (2017), 1703.00187.
- [55] L. Bian et al., *Sci. China Phys. Mech. Astron.* **64**, 120401 (2021), 2106.10235.
- [56] R.-G. Cai and T. Yang, *Phys. Rev. D* **95**, 044024 (2017), 1608.08008.
- [57] R.-G. Cai, T.-B. Liu, X.-W. Liu, S.-J. Wang, and T. Yang, *Phys. Rev. D* **97**, 103005 (2018), 1712.00952.
- [58] R.-G. Cai and T. Yang, *EPJ Web Conf.* **168**, 01008 (2018), 1709.00837.
- [59] X. Zhang, *Sci. China Phys. Mech. Astron.* **62**, 110431 (2019), 1905.11122.
- [60] H.-Y. Chen, *Phys. Rev. Lett.* **125**, 201301 (2020), 2006.02779.
- [61] W. Zhao, C. Van Den Broeck, D. Baskaran, and T. G. F. Li, *Phys. Rev. D* **83**, 023005 (2011), 1009.0206.
- [62] M. Du, W. Yang, L. Xu, S. Pan, and D. F. Mota, *Phys. Rev. D* **100**, 043535 (2019), 1812.01440.
- [63] W. Yang, S. Pan, E. Di Valentino, B. Wang, and A. Wang, *JCAP* **05**, 050 (2020), 1904.11980.
- [64] R. R. A. Bacheaga, A. A. Costa, E. Abdalla, and K. S. F. Fornazier, *JCAP* **05**, 021 (2020), 1906.08909.
- [65] Z. Chang, Q.-G. Huang, S. Wang, and Z.-C. Zhao, *Eur. Phys. J. C* **79**, 177 (2019).
- [66] J.-h. He, *Phys. Rev. D* **100**, 023527 (2019), 1903.11254.
- [67] Z.-W. Zhao, L.-F. Wang, J.-F. Zhang, and X. Zhang, *Sci. Bull.* **65**, 1340 (2020), 1912.11629.
- [68] L.-F. Wang, Z.-W. Zhao, J.-F. Zhang, and X. Zhang, *JCAP* **11**, 012 (2020), 1907.01838.
- [69] J.-Z. Qi, S.-J. Jin, X.-L. Fan, J.-F. Zhang, and X. Zhang, *JCAP* **12**, 042 (2021), 2102.01292.
- [70] S.-J. Jin, L.-F. Wang, P.-J. Wu, J.-F. Zhang, and X. Zhang, *Phys. Rev. D* **104**, 103507 (2021), 2106.01859.
- [71] T. Zhu, W. Zhao, and A. Wang (2022), 2210.05259.
- [72] J. M. S. de Souza, R. Sturani, and J. Alcaniz, *JCAP* **03**, 025 (2022), 2110.13316.
- [73] L.-F. Wang, S.-J. Jin, J.-F. Zhang, and X. Zhang, *Sci. China Phys. Mech. Astron.* **65**, 210411 (2022), 2101.11882.
- [74] P.-J. Wu, Y. Shao, S.-J. Jin, and X. Zhang (2022), 2202.09726.
- [75] S.-J. Jin, R.-Q. Zhu, L.-F. Wang, H.-L. Li, J.-F. Zhang, and X. Zhang, *Commun. Theor. Phys.* **74**, 105404 (2022), 2204.04689.
- [76] W.-T. Hou, J.-Z. Qi, T. Han, J.-F. Zhang, S. Cao, and X. Zhang (2022), 2211.10087.
- [77] M. Califano, I. de Martino, D. Vernieri, and S. Capozziello (2022), 2208.13999.
- [78] L.-F. Wang, Y. Shao, G.-P. Zhang, J.-F. Zhang, and X. Zhang (2022), 2201.00607.
- [79] A. Dhani, S. Borhanian, A. Gupta, and B. Sathyaprakash (2022), 2212.13183.
- [80] E. O. Colgáin, in *17th Italian-Korean Symposium on Relativistic Astrophysics* (2022), 2203.03956.
- [81] M.-D. Cao, J. Zheng, J.-Z. Qi, X. Zhang, and Z.-H. Zhu, *Astrophys. J.* **934**, 108 (2022), 2112.14564.
- [82] X. Fu, L. Zhou, J. Yang, Z.-Y. Lu, Y. Yang, and G. Tang, *Chin. Phys. C* **45**, 065104 (2021).
- [83] C. Ye and M. Fishbach, *Phys. Rev. D* **104**, 043507 (2021), 2103.14038.
- [84] H.-Y. Chen, P. S. Cowperthwaite, B. D. Metzger, and E. Berger, *Astrophys. J. Lett.* **908**, L4 (2021), 2011.01211.
- [85] S.-J. Jin, T.-N. Li, J.-F. Zhang, and X. Zhang (2022), 2202.11882.
- [86] A. Mitra, J. Mifsud, D. F. Mota, and D. Parkinson, *Mon. Not. Roy. Astron. Soc.* **502**, 5563 (2021), 2010.00189.
- [87] N. B. Hogg, M. Martinelli, and S. Nesseris, *JCAP* **12**, 019 (2020), 2007.14335.
- [88] R. C. Nunes, *Phys. Rev. D* **102**, 024071 (2020), 2007.07750.

- [89] S.-J. Jin, S.-S. Xing, Y. Shao, J.-F. Zhang, and X. Zhang (2023), 2301.06722.
- [90] S. Borhanian, A. Dhani, A. Gupta, K. G. Arun, and B. S. Sathyaprakash, *Astrophys. J. Lett.* **905**, L28 (2020), 2007.02883.
- [91] B. P. Abbott et al. (LIGO Scientific), *Class. Quant. Grav.* **34**, 044001 (2017), 1607.08697.
- [92] M. Punturo et al., *Class. Quant. Grav.* **27**, 194002 (2010).
- [93] M. Evans et al. (2021), 2109.09882.
- [94] S.-J. Jin, D.-Z. He, Y. Xu, J.-F. Zhang, and X. Zhang, *JCAP* **03**, 051 (2020), 2001.05393.
- [95] J. Yu, H. Song, S. Ai, H. Gao, F. Wang, Y. Wang, Y. Lu, W. Fang, and W. Zhao, *Astrophys. J.* **916**, 54 (2021), 2104.12374.
- [96] E. Belgacem, Y. Dirian, S. Foffa, E. J. Howell, M. Maggiore, and T. Regimbau, *JCAP* **08**, 015 (2019), 1907.01487.
- [97] M. Safarzadeh, E. Berger, K. K. Y. Ng, H.-Y. Chen, S. Vitale, C. Whittle, and E. Scannapieco, *Astrophys. J. Lett.* **878**, L13 (2019), 1904.10976.
- [98] J.-F. Zhang, H.-Y. Dong, J.-Z. Qi, and X. Zhang, *Eur. Phys. J. C* **80**, 217 (2020), 1906.07504.
- [99] X.-N. Zhang, L.-F. Wang, J.-F. Zhang, and X. Zhang, *Phys. Rev. D* **99**, 063510 (2019), 1804.08379.
- [100] J.-F. Zhang, M. Zhang, S.-J. Jin, J.-Z. Qi, and X. Zhang, *JCAP* **09**, 068 (2019), 1907.03238.
- [101] W.-H. Ruan, Z.-K. Guo, R.-G. Cai, and Y.-Z. Zhang, *Int. J. Mod. Phys. A* **35**, 2050075 (2020), 1807.09495.
- [102] Y.-L. Wu, *Int. J. Mod. Phys. A* **33**, 1844014 (2018), 1805.10119.
- [103] W.-R. Hu and Y.-L. Wu, *Natl. Sci. Rev.* **4**, 685 (2017).
- [104] S. Liu, Y.-M. Hu, J.-d. Zhang, and J. Mei, *Phys. Rev. D* **101**, 103027 (2020), 2004.14242.
- [105] H.-T. Wang et al., *Phys. Rev. D* **100**, 043003 (2019), 1902.04423.
- [106] J. Luo et al. (TianQin), *Class. Quant. Grav.* **33**, 035010 (2016), 1512.02076.
- [107] J. Luo et al., *Class. Quant. Grav.* **37**, 185013 (2020), 2008.09534.
- [108] V. K. Milyukov, *Astron. Rep.* **64**, 1067 (2020).
- [109] J. Mei et al. (TianQin), *PTEP* **2021**, 05A107 (2021), 2008.10332.
- [110] T. Robson, N. J. Cornish, and C. Liu, *Classical and Quantum Gravity* **36**, 105011 (2019), 1803.01944.
- [111] P. Amaro-Seoane et al. (LISA) (2017), 1702.00786.
- [112] P. Auclair et al. (LISA Cosmology Working Group) (2022), 2204.05434.
- [113] C. Palenzuela, L. Lehner, and S. L. Liebling, *Science* **329**, 927 (2010), 1005.1067.
- [114] R. O’Shaughnessy, D. L. Kaplan, A. Sesana, and A. Kamble, *Astrophys. J.* **743**, 136 (2011), 1109.1050.
- [115] P. Moesta, D. Alic, L. Rezzolla, O. Zanotti, and C. Palenzuela, *Astrophys. J. Lett.* **749**, L32 (2012), 1109.1177.
- [116] D. L. Kaplan, R. O’Shaughnessy, A. Sesana, and M. Volonteri, *Astrophys. J. Lett.* **734**, L37 (2011), 1105.3653.
- [117] J.-M. Shi, J. H. Krolik, S. H. Lubow, and J. F. Hawley, *Astrophys. J.* **749**, 118 (2012), 1110.4866.
- [118] R. D. Blandford and R. L. Znajek, *Mon. Not. Roy. Astron. Soc.* **179**, 433 (1977).
- [119] D. L. Meier, *Astrophys. J. Lett.* **548**, L9 (2001), astro-ph/0010231.
- [120] M. Dotti, A. Sesana, and R. Decarli, *Adv. Astron.* **2012**, 940568 (2012), 1111.0664.
- [121] *SKA*, <http://www.skatelescope.org>.
- [122] *ELT*, <http://www.eso.org/sci/facilities/eelt/>.
- [123] *LSST*, <http://www.lsst.org>.
- [124] R.-G. Cai, Z.-K. Guo, B. Hu, C. Liu, Y. Lu, W.-T. Ni, W.-H. Ruan, N. Seto, G. Wang, and Y.-L. Wu (2023), 2305.04551.
- [125] R. Wang, W.-H. Ruan, Q. Yang, Z.-K. Guo, R.-G. Cai, and B. Hu, *Natl. Sci. Rev.* **9**, nwab054 (2022), 2010.14732.
- [126] W.-H. Ruan, C. Liu, Z.-K. Guo, Y.-L. Wu, and R.-G. Cai (2019), 1909.07104.
- [127] W.-H. Ruan, C. Liu, Z.-K. Guo, Y.-L. Wu, and R.-G. Cai, *Nature Astron.* **4**, 108 (2020), 2002.03603.
- [128] L.-G. Zhu, L.-H. Xie, Y.-M. Hu, S. Liu, E.-K. Li, N. R. Napolitano, B.-T. Tang, J.-d. Zhang, and J. Mei, *Sci. China Phys. Mech. Astron.* **65**, 259811 (2022), 2110.05224.
- [129] L.-G. Zhu, Y.-M. Hu, H.-T. Wang, J.-d. Zhang, X.-D. Li, M. Hendry, and J. Mei, *Phys. Rev. Res.* **4**, 013247 (2022), 2104.11956.
- [130] W.-F. Feng, H.-T. Wang, X.-C. Hu, Y.-M. Hu, and Y. Wang, *Phys. Rev. D* **99**, 123002 (2019), 1901.02159.
- [131] T. Robson, N. J. Cornish, and C. Liu, *Class. Quant. Grav.* **36**, 105011 (2019), 1803.01944.
- [132] A. Buonanno, B. Iyer, E. Ochsner, Y. Pan, and B. S. Sathyaprakash, *Phys. Rev. D* **80**, 084043 (2009), 0907.0700.
- [133] A. Krolak, K. D. Kokkotas, and G. Schaefer, *Phys. Rev. D* **52**, 2089 (1995), gr-qc/9503013.
- [134] E. Belgacem et al. (LISA Cosmology Working Group), *JCAP* **07**, 024 (2019), 1906.01593.
- [135] C. M. Hirata, D. E. Holz, and C. Cutler, *Phys. Rev. D* **81**, 124046 (2010), 1004.3988.
- [136] N. Tamanini, C. Caprini, E. Barausse, A. Sesana, A. Klein, and A. Petiteau, *JCAP* **04**, 002 (2016), 1601.07112.
- [137] B. Kocsis, Z. Frei, Z. Haiman, and K. Menou, *Astrophys. J.* **637**, 27 (2006), astro-ph/0505394.
- [138] L. Speri, N. Tamanini, R. R. Caldwell, J. R. Gair, and B. Wang, *Phys. Rev. D* **103**, 083526 (2021), 2010.09049.
- [139] T. Dahlen et al., *Astrophys. J.* **775**, 93 (2013), 1308.5353.
- [140] O. Ilbert et al., *Astron. Astrophys.* **556**, A55 (2013), 1301.3157.
- [141] E. Barausse, *Mon. Not. Roy. Astron. Soc.* **423**, 2533 (2012), 1201.5888.
- [142] S. A. e. a. Klein A, Barausse E, *Phys Rev D* **93**, 024003 (2016), 1511.05581.
- [143] P. Madau and M. J. Rees, *Astrophys. J. Lett.* **551**, L27 (2001), astro-ph/0101223.
- [144] M. Volonteri, G. Lodato, and P. Natarajan, *Mon. Not. Roy. Astron. Soc.* **383**, 1079 (2008), 0709.0529.
- [145] M. Volonteri, F. Haardt, and P. Madau, *Astrophys. J.* **582**, 559 (2003), astro-ph/0207276.
- [146] P. A. Seoane et al., *Gen. Rel. Grav.* **54**, 3 (2022), 2107.09665.
- [147] R. Gold, V. Paschalidis, M. Ruiz, S. L. Shapiro, Z. B. Etienne, and H. P. Pfeiffer, *Phys. Rev. D* **90**, 104030 (2014), 1410.1543.
- [148] B. D. Farris, P. Duffell, A. I. MacFadyen, and Z. Haiman, *Mon. Not. Roy. Astron. Soc.* **447**, L80 (2015), 1409.5124.

- [149] D. George and E. A. Huerta, Phys. Lett. B **778**, 64 (2018), 1711.03121.
- [150] D. George and E. A. Huerta, Phys. Rev. D **97**, 044039 (2018), 1701.00008.
- [151] T. D. Gebhard, N. Kilbertus, I. Harry, and B. Schölkopf, Phys. Rev. D **100**, 063015 (2019), 1904.08693.
- [152] *SKA1 system baseline design v2*, [https://www.skao.int/sites/default/files/documents/d1-SKA-TEL-SKO-0000002\\_03\\_SKA1SystemBaselineDesignV2\\_1.pdf](https://www.skao.int/sites/default/files/documents/d1-SKA-TEL-SKO-0000002_03_SKA1SystemBaselineDesignV2_1.pdf).
- [153] G. Bruzual and S. Charlot, Mon. Not. Roy. Astron. Soc. **344**, 1000 (2003), astro-ph/0309134.
- [154] R. Davies et al. (MICADO Team), Proc. SPIE Int. Soc. Opt. Eng. **7735**, 77352A (2010), 1005.5009.
- [155] A. Lewis and S. Bridle, Phys. Rev. D **66**, 103511 (2002), astro-ph/0205436.
- [156] L. Chen, Q.-G. Huang, and K. Wang, JCAP **02**, 028 (2019), 1808.05724.
- [157] D. Brout et al., Astrophys. J. **938**, 110 (2022), 2202.04077.